ACS OMEGA

Open Access



http://pubs.acs.org/journal/acsodf

Article

# Low-Viscous, Dilute Phase Adhesive from Dense Polyphenolic Coacervates of Poly(vinyl alcohol) and Tannic acid

Helen H. Ju, Eunu Kim, Han-Yeol Yang, Yu Ri Nam, Jingxian Wu, and Haeshin Lee*

Cite This: *ACS Omega* 2024, 9, 2953−2961

Read Online

ACCESS | Metrics & More | Article Recommendations | Supporting Information

**ABSTRACT:** This study explores a polyphenolic coacervate, named VATA, formed by poly(vinyl alcohol) (PVA) and tannic acid (TA). Distinct from conventional studies that have focused on the bottom, dense phase of coacervates, this research emphasizes the top, dilute phase, low-viscous coacervate liquid termed liquid-VATA (*l*-VATA). Due to TA's capability of intermolecular association as well as adhesiveness, phenomena not typically observed in the upper dilute phase of standard polyelectrolyte-based coacervates are revealed. At first glance, the dilute phase *l*-VATA coacervate resembles a water-like, low-viscous mixture solution of PVA, TA, and PVA/TA complexes. However, analysis shows that nearly all of the TA molecules associate with PVA chains, forming PVA/TA complexes. Furthermore, supraparticular association was observed between PVA/TA complex nanoparticles upon applying external shear force. A broad survey of shear rate and strain showed that the solution exhibited sequential shear-thickening, followed by shear-thinning behavior. The water-like, low viscosity of *l*-VATA unexpectedly reveals robust adhesiveness and thus able to lift an entire mouse using just a single human hair strand. Even in cases of failure, no interfacial failure was detected between mouse and human hair. In addition to enabling hair-to-hair bonding, our study also showcases the efficacy of *l*-VATA in facilitating hair-to-skin adhesion. The results illustrate how the lower viscosity of *l*-VATA can be exploited for a wide range of industrial and cosmetic applications, allowing the formulation of thin, uniform adhesive layers, something unachievable with the dense, viscous VATA glue. Thus, this study highlights the importance of investigating the top dilute phase of coacervates, shedding light on an area often underestimated compared to the bottom dense phase reported in prevalent coacervate studies.

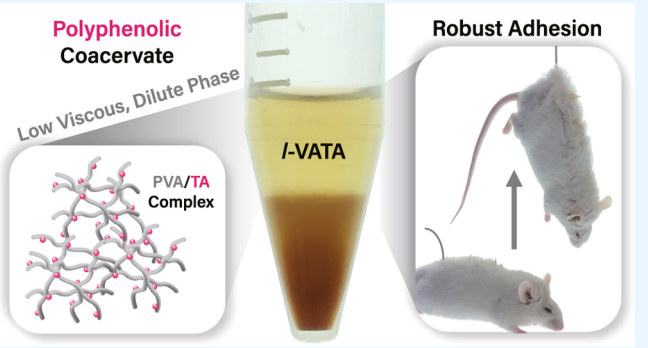


## 1. INTRODUCTION

The scientific intrigue about coacervates − concentrated droplets generated from liquid-to-liquid phase separation − has drawn much attention since the first recognition in 1929.[1] These fuzzy yet fascinating entities, in the context of biology, serve as membraneless compartments within cells, providing a spatiotemporal platform for a plethora of biochemical reactions. On the contrary, synthetic polyelectrolyte coacervates have been reported with a myriad of applications extending beyond the realm of biology. Leveraging their distinct physicochemical properties, they contribute to the synthesis of nanomaterials,[2] drug delivery systems,[3] cosmetic formulations,[4] and enhancements in food processing.[5]

Looking closely at the underlying thermodynamics, we see that coacervates are dynamic systems primarily controlled by chemical equilibrium. The creation of complex coacervates from synthetic polymers largely depends on the interactions between cationic and anionic polymers, which is a process of electrostatic bindings. Notable instances involve coacervate formations among poly(allylamine hydrochloride) (PAH)/poly(acrylic acid) (PAA),[6] polyethylenimine (PEI)/PAA,[7] poly(diallyldimethylammonium chloride) (PDADMAC)/poly(styrenesulfonate) (PSS),[8] and many others. More recently, neutral, polyphenolic coacervate systems have emerged.[9−12] The polyphenolic coacervates are formed by hydrogen bond basis.[13−15] These coacervates stand out due to their adhesive properties, unveiling a molecular mechanism reminiscent of mussel adhesion.[16] Moreover, a coacervate formed by combination of electrostatic (i.e., cationic) and hydrogen bonding prepared by poly(amidoamine-epichlorohydrin) (PAE) and tannic acid was reported.[17] This synergistic hybrid phenolic and cationic polymer provides a reusable adhesive.

Nearly all coacervate studies have focused on the bottom, concentrated phase. Yet, the upper liquid (i.e., the dilute phase), consistently in equilibrium with the bottom coacervate, holds scientific significance deserving equal attention but has tradi-

Received: November 7, 2023
Revised: December 19, 2023
Accepted: December 21, 2023
Published: December 29, 2023

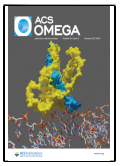

tionally been overlooked. While there have been studies by introducing a third-party substance, such as salt or poly(ethylene glycol) (PEG), into the dilute phase to alter the characteristics of the underlying dense coacervate phase, investigations into the inherent function of the dilute phase itself remain scarce.[18,19] Recently, researchers examined the role of a phenolic catechol moiety as a third-party client molecule in coacervates. Findings indicate that the catechol preferentially partitions into the dense coacervate phase, which in turn serves as a redox insulator, effectively protecting the catechol from oxidation.[16,20] Thus, our study aims to fill this gap by presenting the innate functions and various applications of diluted coacervates, thereby introducing the idea that the upper dilute phase of the coacervate also holds functional importance. Characterized by low polymer concentrations and viscosity, this phase nevertheless maintains the inherent properties of its counterpart of the dense coacervate.[21] This realization might serve to broaden our understanding of coacervate behavior and functions, extending beyond the condensed state. In particular, the low viscosity of polyphenolic adhesive coacervates offers a distinct advantage over dense bottom phase adhesive, as it allows for facile handling and enables application of thin, uniform layers on biological surfaces such as hair and skin.

Herein, we report the unique physicochemical behavior and functional characteristics of the upper dilute phase of polyphenolic coacervates, formed by poly(vinyl alcohol) (PVA) and tannic acid (TA), which is termed VATA. Instead of focusing on the dense, bottom coacervate of VATA, this study explores the physicochemical properties and applications of the spontaneously generated, water-like upper phase called liquid-VATA (*l*-VATA) after aqueous-to-aqueous phase separation. The composition ratio of *l*-VATA (PVA:TA = ∼ 6:1 wt %) closely resembles that of the corresponding dense bottom phase (5:1 wt %), with all TA molecules associating with PVA chains. A noticeable feature of *l*-VATA is its shear response behavior. Interparticular associations between PVA/TA complex nanoparticles were observed upon applying external shear force. Extensive rheological experiments on shear rate and strain revealed that *l*-VATA exhibits sequential shear-thickening, followed by shear-thinning behavior. Despite *l*-VATA's low viscosity, its adhesion strength is sufficiently robust to lift the entire body of a mouse using a single hair strand attachment. In addition to facilitating hair-to-hair bonding, *l*-VATA demonstrates an effective adhesive strength for hair-to-skin adhesion, as well. Our experiments indicate that the lower viscosity of *l*-VATA makes it particularly suited for diverse industrial and cosmetic applications, allowing for the formation of a thin, uniform adhesive layer − something unattainable with the dense, viscous VATA glue formed in the bottom phase. Our study underscores the significance of investigating the upper dilute phase of adhesive coacervates, extending beyond polyphenolic systems to general polyelectrolyte ones as well.

## 2. EXPERIMENTAL SECTION

**2.1. Materials.** Poly(vinyl alcohol) (PVA) (average molecular weight = 13−23 kDa, 87−89% hydrolyzed), tannic acid (TA) (molecular weight = 1701.2 Da isolated from Chinese natural gall nuts), and poly(ethylene glycol) (molecular weight = 2, 4, 10, 20, and 35 kDa) were purchased from Sigma-Aldrich. Sodium chloride (NaCl) was purchased from Duchefa Biochemie. Hair strips were purchased from Pinktreedapam (Korea), and ICR mice were purchased from Orient Bio (Korea).

**2.2. *l*-VATA Preparation.** PVA and TA were separately dissolved in a double-distilled water (DDW). PVA was dissolved by stirring the solution at 85 °C for 24 h. The final concentration of TA was 4 wt %, and that of PVA was 20 wt %. PVA (5 mL) and TA (5 mL) solutions were mixed, and the mixture was vigorously shaken for 10 s. At this step, the liquid-to-liquid phase separation can be observed. There are two methods to prepare dense and dilute coacervates. One is to leave the PVA/TA mixture under an ambient condition for 48 h, allowing gradual generation of dense coacervate phase (bottom) and the corresponding dilute phase (top). The other is to centrifuge the mixture at 3000 rpm for 20 min. The second approach should be followed by leaving the solution under an ambient condition for at least 24 h for stabilization.

**2.3. Determination of PVA and TA Compositions in a Dilute Phase.** To determine the amount of PVA in a dilute phase of the PVA/TA coacervate system, a gel permeable chromatography (GPC) experiment was conducted on an Agilent 1260 Infinity system (Santa Clara, CA, USA) using a 0.1 M NaCl solution in double-distilled water (DDW) as a mobile phase. The GPC column employed was an OHpak SB-804 HQ (Shodex). The GPC system was equipped with a 1260 refractive index detector and a UV detector. Prior to analysis, all samples (PVA, TA, and *l*-VATA) were diluted in DDW, and each 20 $\mu$L sample was injected. The GPC analysis ran for a duration of 30 min at 25 °C. Peak integration was performed using established PVA standard curves, represented by the equation $y = 6.49 - (-0.39) * \ln(x - 0.09)$, where $x$ denotes the PVA amount (wt %), and $y$ corresponds to the peak integration value.

To determine the amount of TA in a dilute phase of the PVA/TA coacervate, a UV−vis spectrophotometer was employed. The *l*-VATA solutions were then subjected to absorbance measurements at 280 nm using the diode array of a UV−vis spectrophotometer (HP8453, Hewlett-Packard, USA). Tannic acid standard curves, represented by the equation $y = -0.22 + 18.88x$, were generated in the range of 0.025−0.125 wt %.

**2.4. DLS Experiments.** To study the physical behavior of PVA/TA complexes in a dilute phase, we applied external shear force to the solution, and the change in size by complex association was determined by dynamic light scattering (DLS) (ELSZ-2000, Otsuka). A volume of 2 mL of 1/100 diluted *l*-VATA solutions in a 15 mL conical tube underwent five cycles of 10 s vortexing (2500 rpm) followed by 5 min of stabilization. After stabilization, the size of complexes was measured by DLS at the end of each cycle (total five times).

**2.5. AFM Imaging.** For tapping-mode atomic force microscopy (AFM) analysis (FX-40; Park Systems), a freshly cleaned silicon substrate was utilized. A volume of 100 $\mu$L of 1/100 diluted *l*-VATA solutions (pre- and post-shear force application) was drop-cast onto the silicon surface and allowed to stand for 5 min. During this time, dilute PVA/TA complexes were adsorbed onto the surface. Subsequently, the silicon surfaces were rinsed with distilled water three times. A silicon SPM sensor (NCHR-50, Nanosensors) cantilever with a resonance frequency of 320 kHz was employed for tuning. During the imaging process, a scan size of 10 × 10 $\mu m^2$ was selected with a scan rate set to 0.3 Hz. Following imaging, the XEI program (Threshold 2.0 − Upper range, 0.200 nm) was employed for quantitative analysis of the individual particle volume.

**2.6. Adhesion Strength Measurement with UTM.** To measure the tensile strength before and after the shear application of the *l*-VATA solution, universal testing machine


https://doi.org/10.1021/acsomega.3c08833
ACS Omega 2024, 9, 2953−2961

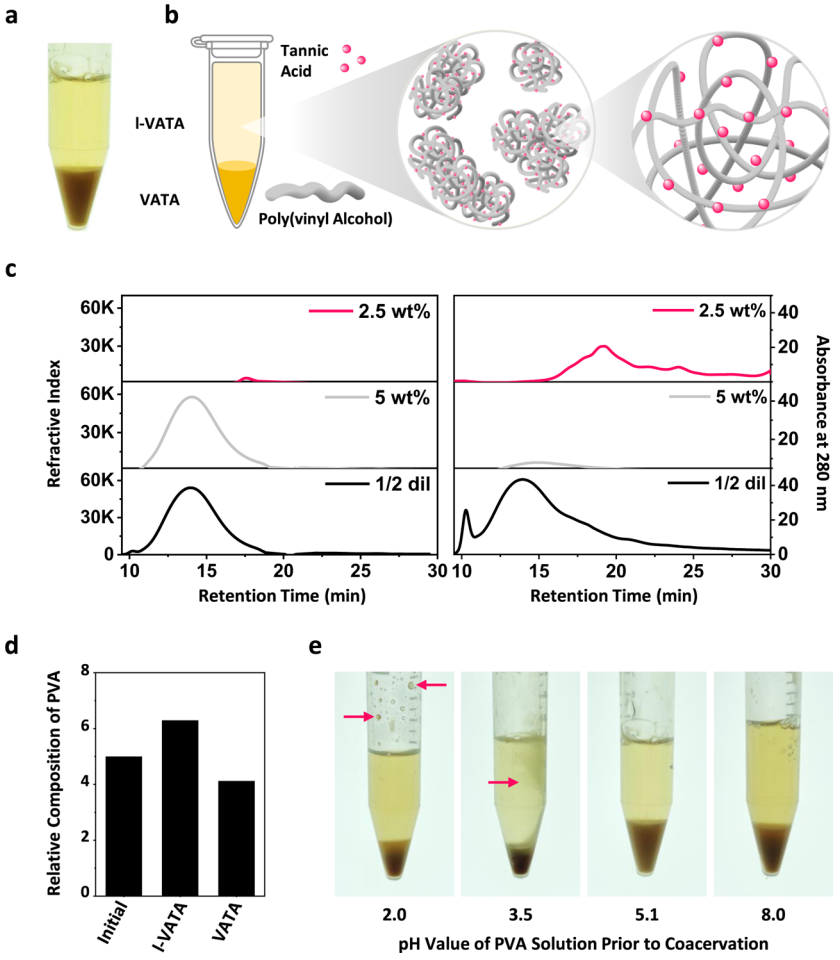


**Figure 1.** Formation and spontaneous phase separation of VATA and *l*-VATA. (a) Photograph of the two phases of the VATA coacervate. (b) Schematic description of the PVA/TA complex (a gray line represents PVA and a pink sphere does TA) in *l*-VATA phase. (c) GPC chromatograms coupled with RI detector (left; TA (pink, top), PVA (gray, middle), and *l*-VATA (black, bottom)) and with UV detector (right; TA (top), PVA (middle), and *l*-VATA (bottom)). (d) Compositions of PVA relative to that of TA in the initial PVA and TA solutions, before mixing (left), *l*-VATA (middle), and bottom VATA phase (right) ($n = 3$). (e) Photographs of VATA coacervate formations as a function of pH values of the PVA solution. Pink arrows indicate the adhesion of VATA formed in progress of coacervate formation, resisting against centrifugal force.

(UTM) was employed. 200 $\mu$L of the *l*-VATA solution was applied onto a wooden popsicle stick (cross-sectional area = 3.8 $cm^2$). Excessive amount of the solution was trimmed and then dried under ambient condition for 3 h. The force was applied with a 500 N load cell at a controlled rate (300 mm $min^{-1}$) to the specimen until the two popsicles detach, at which point the force was recorded. The tensile strength (MPa) of the samples was calculated by dividing the maximum load (N) by the cross-sectional area.

**2.7. Rheological Properties of *l*-VATA.** Rheological properties of *l*-VATA were measured by using a conventional rheometer (MCR 302, Anton Paar) with a parallel plate geometry (0.5 mm gap, 25 mm diameter). Two different modes (amplitude sweep and shear viscosity) of an oscillatory shear rheology were applied for measuring rheological properties of *l*-VATA. In an amplitude sweep mode, shear moduli at a fixed frequency (1 rad $s^{-1}$) were measured with shear strain ($\gamma$) ranging from 10 to 6000%. The shear viscosity of 14 wt % PVA or *l*-VATA solution was measured in continuous flow with shear rates from 10 to 1000 $s^{-1}$.

**2.8. Cell Viability Test.** L929 cells ($1 \times 10^4$ cells/well) were seeded in 96-well plates with Dulbecco's Modified Eagle Medium (pH 7.4, Gibco; Thermo Fisher Scientific, Inc., Waltham, MA, USA) supplemented with 10 vol % fetal bovine serum and 1 vol % penicillin-streptomycin. The cells were incubated at 37 °C under a 5% $CO_2$ environment for 24 h. For the cytotoxicity test, *l*-VATA solution and controls — 10.15% PVA, 1.62% TA, and 1× phosphate-buffered saline (PBS, pH 7.4, Gibco; Thermo Fisher Scientific, Inc., Waltham, MA, USA) — were prewarmed to 37 °C. Various sample volumes (0.25, 0.5, 1, and 1.5 $\mu$L) were added to each well. After 24-h exposure, cytotoxicity was assessed via both qualitative (LIVE/DEAD) and quantitative (CCK-8) methods. For qualitative analysis, the culture media were removed, and cells were stained with calcein AM (2 $\mu$M) and ethidium homodimer (4 $\mu$M) from the LIVE/DEAD Viability/Cytotoxicity Kit (Invitrogen, Carlsbad, CA, USA) for 20 min in Dulbecco's phosphate-buffered saline (DPBS). Fluorescence images were obtained using an Eclipse Ti fluorescence microscope (Nikon, Tokyo, Japan). For quantitative analysis, the culture media were replaced with 100 $\mu$L of fresh complete media containing 10 $\mu$L of the cell counting kit-8 (CCK-8). After 1 h of incubation at 37 °C under a 5% $CO_2$ environment, the absorbance at 450 nm was measured using a Varioskan Flash reader (Thermo Fisher Scientific Inc., Waltham, MA, USA). All experiments were conducted in triplicate, and


https://doi.org/10.1021/acsomega.3c08833
ACS Omega 2024, 9, 2953−2961

cell viability was calculated according to the International Organization for Standardization (ISO) 10993-5 guidelines.

**2.9. Hair-to-Hair Extension.** In the weight lifting experiment, *l*-VATA was loaded into an 18G needle, and a single strand of hair was threaded into a 30G needle, leaving 3 cm of hair exposed. The hair strand was immersed in *l*-VATA for 1 min, after which the two strands of dipped hair were glued together in opposite directions. Ten sets of glued hair strands were prepared for the weight lifting experiment.

**2.10. Hair Extension Application with ICR Mouse.** A volume of 20 $\mu$L of *l*-VATA was loaded into a pipette tip, which was then threaded with a single strand of hair cut to a length of 2 cm. Approximately 0.7 cm of the hair strand was adhered to a few strands of ICR mouse hair. The *l*-VATA was allowed to dry for 20 min, after which the mouse was lifted by holding onto the hair strand. All animals received humane care in accordance with the Guide for the Care and Use of Laboratory Animals published by the National Institutes of Health, and all animal experiments were approved by the KAIST Institutional Animal Care and Use Committee.

**2.11. Hair-to-Skin Attachment Application.** A 10 × 15 cm piece of pork skin was prepared and heated to 37 °C in a water bath. The tips of seven human hair strands were dipped into the *l*-VATA and then attached to the pork skin. The *l*-VATA and the attached hairs were cured under ambient conditions for 5 min. After curing, tweezers were used to apply mechanical stress by sliding back and forth, touching the top tips of the hair strands. To further evaluate *l*-VATA's adhesive strength stability against water, three drops of water were applied to the adhered area, followed by repeating the tweezing motion five times.

**2.12. Statistical Analysis.** All numerical data were analyzed using OriginPro 9.6 (OriginLab) by one-way ANOVA and are presented as means ± standard deviation values. The $p$ value was considered significantly different at 0.05 level ($^{*}p < 0.05$, $^{**}p < 0.01$, and $^{***}p < 0.001$).

## 3. RESULTS AND DISCUSSION

The VATA coacervate was prepared by the following method. A PVA solution (20 wt %) and a TA solution (4 wt %) were prepared in distilled water and then mixed in a volume ratio of 1:1. At this stage, an opaque coacervate complex dispersed in water was observed with the naked eye. There are two ways to separate the dense phase (VATA) and the dilute phase (liquid-VATA, *l*-VATA). The first method is to leave the turbid VATA solution under ambient conditions for 48 h. The second method is to accelerate the above process by centrifuging at 3000 rpm for 20 min and then leaving it under ambient conditions for 24 h. After this, an aqueous-to-aqueous phase separation phenomenon is observed (Figure 1a). In general, since coacervates are in a thermodynamic equilibrium status, the components of the settle down dense phase and the ones of the dilute phase corresponding to the upper layer are closely similar. Thus, we expect that PVA and TA will be present in the dilute phase, *l*-VATA.

The addition of TA imparts adhesive properties to various polymers such as PEG[12] and PEI.[22] Before being mixed, each component, PVA and TA, is water soluble; therefore, the formation of the VATA coacervate (the lower phase, Figure 1a) can be understood as a result of the two molecules binding together. However, in the upper layer (the dilute phase), it is uncertain whether PVA and TA exist separately or are associated with each other. We hypothesize that PVA and TA are also physically associated due to TA's adhesive property. If they are associated, this can be detected by connecting a refractive index (RI) detector and a UV detector in series to the gel permeable chromatography (GPC) system. PVA, being a high-molecular-weight polymer (13−23 kDa), can be detected in the refractive index detector, while TA, a small molecule (1700 Da), can be detected in the UV detector. Therefore, if PVA and TA are associated, TA will appear at PVA's high molecular weight retention time despite its low molecular weight, manifesting TA's absorption in the range for PVA elution time. Figure 1c demonstrates that the PVA elution time is 14.05 min. It was detected in the RI detector (left chromatogram, second row) but not in the UV detector. For TA, the elution time is 19.19 min, and it was detected in the UV detector but not in the RI detector (right chromatogram, first row). In the case of the *l*-VATA mixture, there was a noticeable shift in the UV detector profile, with elution peaks upshifting to 10.27 and 13.95 min. This shift aligns well with the RI detector's results for the PVA profile, appearing in the high molecular weight range.

Subsequently, we conducted experiments in the dilute phase of *l*-VATA to ascertain the specific composition ratio of PVA and TA. For PVA quantification, we derived its standard equation from the GPC chromatogram, calculating it by obtaining peak integration values from sample with varying PVA concentrations ($y = 6.49 - (0.39) * \ln(x - 0.09)$; where $y$ represents the area under the curve, and $x$ does the molecular weight) (Figure S1a). For TA quantification, we measured absorption (280 nm) using a UV−vis spectrophotometer after preparing TA solutions at different concentrations to create a standard curve ($y = -0.22 + 18.88x$; where $y$ represents the absorption, and $x$ does concentrations) (Figure S1b). This analysis revealed that *l*-VATA consists of 1.62 wt % TA and 10.15 wt % PVA. The approximately 10% concentration of PVA indicates a condition where PVA chains are entangled. As observed in Figure S2, there are findings that PVA exists as polymer coils due to hydrogen bonds between PVA interchain starting from around 6 wt % PVA.[23] Thus, TA molecules are associated in the entangled PVA chains in *l*-VATA according to the results, resulting in the representation of the scheme in Figure 1b. Quantitative analysis showed that the composition of the upper *l*-VATA phase was at a PVA:TA ratio of 6.29:1, and that of the bottom phase VATA coacervate was 4.12:1. These ratios are very similar to the initial 5:1 PVA:TA ratio used in creating the coacervate, confirming that the equilibrium status of the liquid-to-liquid phase separation (LLPS) system does exist between the bottom coacervate VATA and the upper dilute phase, *l*-VATA (Figure 1d).

To investigate the influence of the pH on the formation of *l*-VATA, the pH of the PVA solution was adjusted before mixing with the TA solutions. The TA solution's pH was kept constant to preserve the integrity of the hydrolyzable ester bonds. The intrinsic pH value of *l*-VATA was found to be 5.1. When the PVA solution was adjusted to pH 8.0, no significant changes were observed in the morphology of the resulting VATA/*l*-VATA coacervates, as shown in Figure 1e. However, altering the pH of the PVA solution to acidic levels − specifically to pH 3.5 and 2.0 − led to a noticeable increase in the adhesive capabilities of the VATA coacervates. Typically, coacervates formed without pH adjustment settle at the bottom of the tube by centrifugation. In contrast, at the acidic pH, the VATA coacervates struggled to settle, remaining residual adhesive on side walls, which indicates improved adhesive characteristics. This behavior is illustrated in the first two images in Figure 1e. The coacervates, marked by


https://doi.org/10.1021/acsomega.3c08833
ACS Omega 2024, 9, 2953−2961

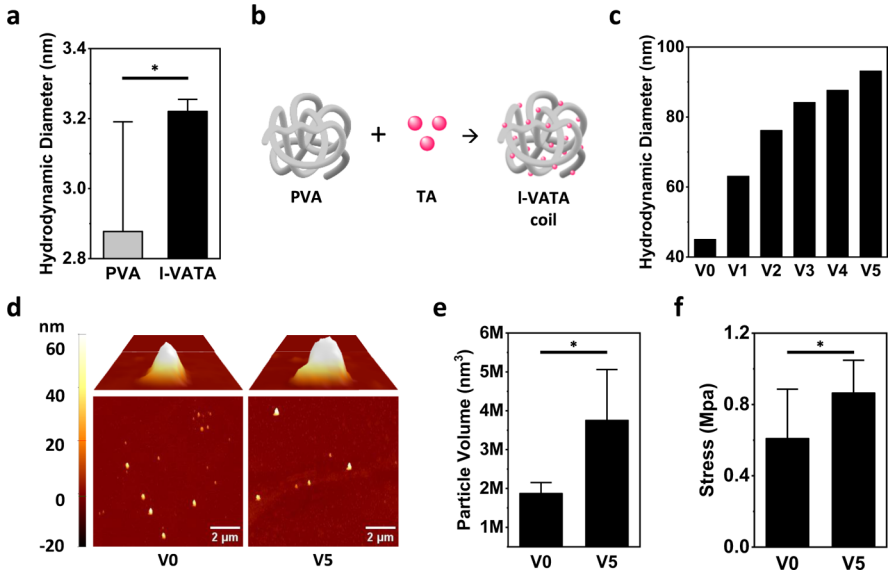


**Figure 2.** Interparticular associations of PVA/TA complexes in *l*-VATA upon responses of external shear force. (a) Hydrodynamic diameters of PVA (left) and *l*-VATA calibrated from GPC result ($n = 4$, $^*p < 0.05$). (b) Schematic representation of TA decoration along PVA chains. (c) DLS results demonstrating hydrodynamic diameter of *l*-VATA increases upon applying shear force ($n = 5$). (d) AFM image of pre- (V0) and post-shear (V5) applied *l*-VATA. (e) Determination of particle volume obtained by AFM results shown in (d) ($n = 4$, $^*p < 0.05$). (f) Adhesion forces of pre- (V0) and post-shear (V5) applied *l*-VATA ($n = 6$, $^*p < 0.05$).

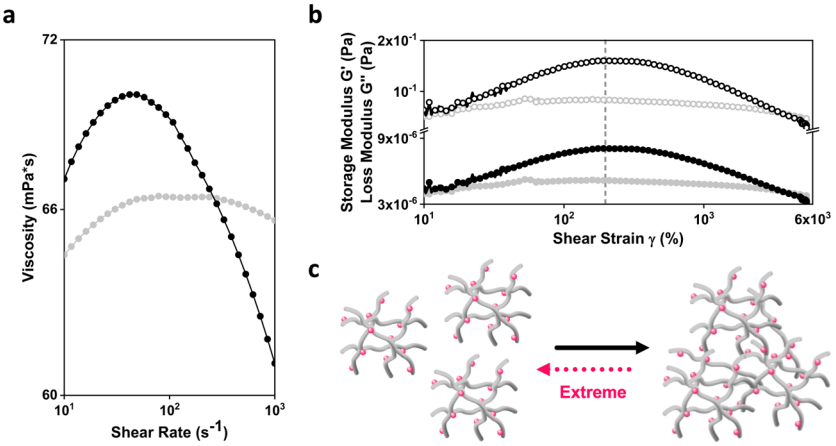


**Figure 3.** Viscosity and rheological behavior of *l*-VATA. (a) Viscosity measurements of 14 wt % PVA (gray) and *l*-VATA solution (black) as a function of shear rate. (b) Changes of storage ($G'$) and loss ($G''$) moduli of PVA ($G'$ = filled gray, $G''$ = empty gray) and *l*-VATA ($G'$ = filled black, $G''$ = empty black). (c) Schematic explanation of the shear-dependent responses shown in (b).

pink arrows, remained suspended or attached on the side wall even after 20 min of centrifugation at 3000 rpm.

The molecular weight of PVA, dissolved in water before forming the coacervate and measured by a GPC elution time, is 12.1 kDa. In contrast, the PVA/TA complex in *l*-VATA measured slightly higher at 12.5 kDa. This was determined by the PEG standard (2, 4, 10, 20, and 35 kDa) (Figure S3). Additionally, the calculated radius of gyration showed a small increase from 2.88 to 3.22 nm (Figure 2a). This change is understood to result from TA decorating and associated with PVA chains (Figure 2b). Consequently, we hypothesized that these decorations by TA might lead to extra intermolecular interactions. To test this, we conducted a simple vortex experiment, using dynamic light scattering (DLS) to measure changes in the hydrodynamic sizes. We vortexed 2 mL of 1/100 diluted *l*-VATA solution for 10 s and then stabilized it at room temperature for 5 min, repeating these five times. At the end of each cycle, we measured the hydrodynamic sizes. The size was indeed gradually increased from 45.02 (V0) nm to 63.1 (V1), 76.1 (V2), 84.1 (V3), 87.6 (V4), and 93.1 (V5) nm after each cycle (Figure 2c). This trend confirmed that the hydrodynamic size grew in response to the external shear force applied through vortexing. Using atomic force microscopy (AFM), we examined the associated status of PVA/TA prior to shear force (V0) and after the fifth vortex cycle (V5). As depicted in Figure 2d, the height and lateral dimension of the particles in the V5 sample exceeded those in the V0 one. When we converted the volume of each particle to equivalent spherical volumes, the V0 sample measured on average $1.9 \times 10^6$ nm$^3$ ($n = 4$) and the V5 sample $3.8 \times 10^6$ nm$^3$ ($n = 4$), reflecting a clear increase (Figure 2e). This evidence allowed us to confirm that the bonding between PVA chains caused by external shear force results in the thickening of the *l*-VATA dilute phase.

Furthermore, the increase in hydrodynamic size at the molecular level due to external shear application might influence the adhesion force. We conducted adhesion stress tests using *l*-



https://doi.org/10.1021/acsomega.3c08833
ACS Omega 2024, 9, 2953−2961

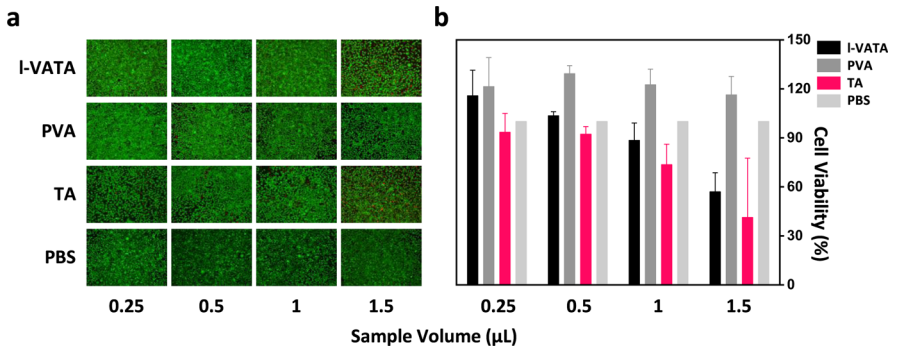


**Figure 4.** Cytotoxicity of *l*-VATA, PVA, and TA on L929 cells. (a) LIVE/DEAD staining (green: live, red: dead) and (b) quantitative cell viability (%) based on the cell counting kit-8 (CCK-8) assay using the undiluted *l*-VATA (black), PVA (gray), TA (pink), and phosphate-buffered saline (PBS) (light gray) ($n$ = 3).

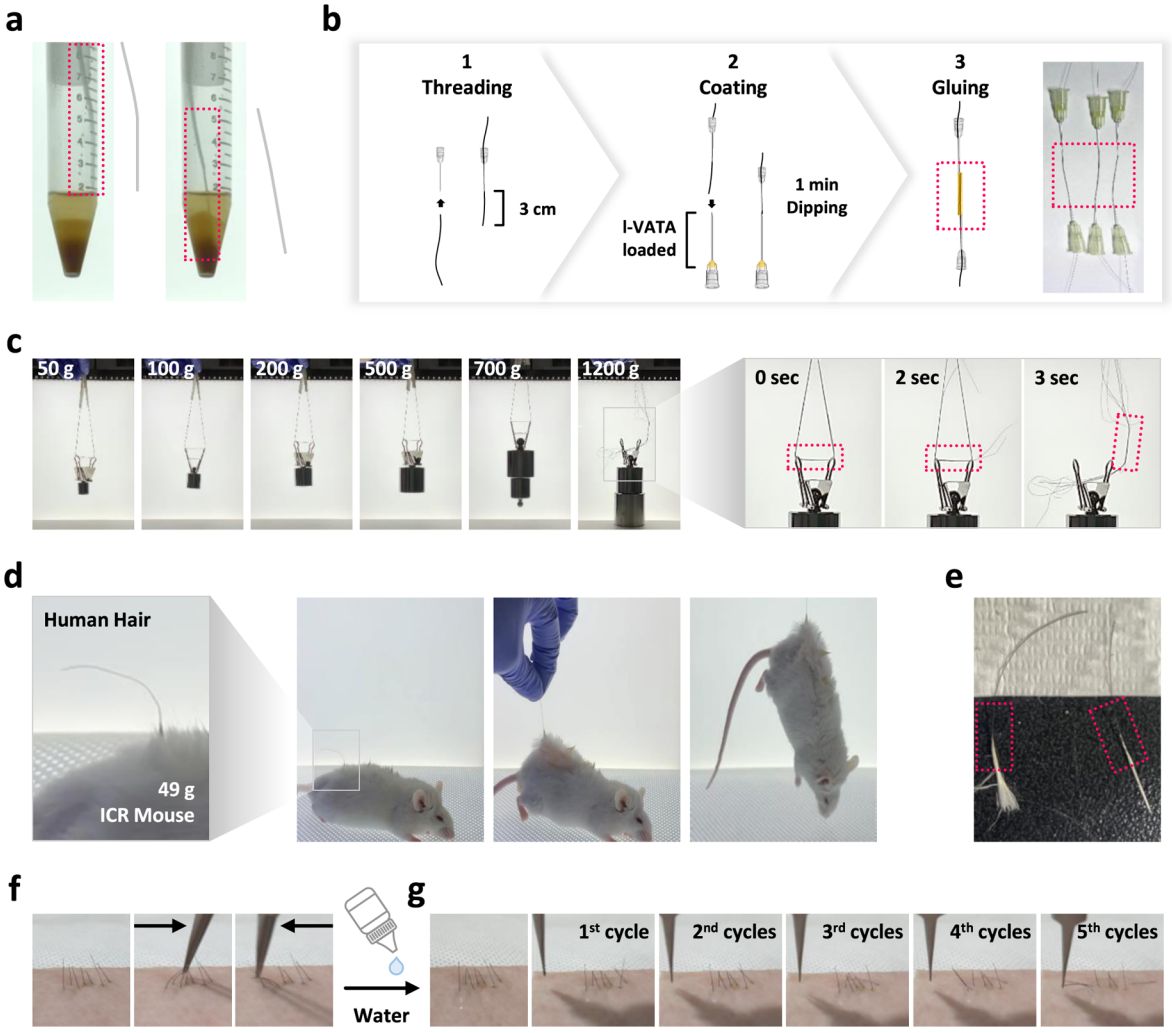


**Figure 5.** Adhesion capability of low viscous *l*-VATA solution. (a) Photographic representation of highly viscous, difficult-to-handle properties of the dense phase of VATA. The bent cable tie (left, red box) can be straightened (right) after dipping and reshaping the bent tie. (b) Schematic description of a needle templated, hair-to-hair gluing method using *l*-VATA. Photographs of (c) weight-lifting demonstration with a fiber consisting of 10 hair strands, (d) a mouse whole body lifting by one strand of human hair, and (e) pulling out of mouse hairs (red box) showing no interfacial failure in the attached regions. Photographs of (f) human hair-to-pork skin attachment and confirmation of adhesion by a tweezers movement. (g) Adhesive strength evaluation in the presence of water.

VATA before, V0, and after, V5, vortexing to measure this effect. Applying 200 $\mu$L of *l*-VATA solution to 3.8 cm$^2$ areas on both ends of two wooden sticks, we joined them and removed the excess *l*-VATA. After a 3 h drying period under ambient conditions, we assessed the adhesive force with the universal testing machine (UTM), applying 500 N of force at 300 mm min$^{-1}$. The results, showcased in Figure 2f, revealed a 71% increase in adhesive force, from 0.61 MPa in the V0 sample to



https://doi.org/10.1021/acsomega.3c08833
ACS Omega 2024, 9, 2953−2961

0.86 MPa after five vortex cycles. Thus, our findings demonstrate that *l*-VATA's adhesion force is augmented when external shear force is applied due to TA-assisted enlargement of polymeric complexes.

One of the key characteristics of the dilute phase located in the upper part of the coacervate is its significantly low viscosity. Considering the results from Figure 2, the polyphenolic coacervate showed a unique increase in hydrodynamic volume and adhesion force through TA-assisted interactions between PVA chains, triggered by shear force. Therefore, we measured the changes in the viscosity of the solution by using a rheometer. Our initial focus was to explore how viscosity responded to different shear rates. By progressively increasing the shear rate from 10 $s^{-1}$ to 1000 $s^{-1}$, we observed that the viscosity of the *l*-VATA continuously increased, reaching a peak at around 43.3 $s^{-1}$. After this point, the viscosity dropped sharply (Figure 3a, black). Such viscosity behavior was weakly observed for PVA only (14 wt %). A slight increase in viscosity was observed until 43.3 $s^{-1}$, then the viscosity was stable until 280 $s^{-1}$, followed by a slight decreased after 280 $s^{-1}$ (Figure 3a, gray). The experiment anticipated that unique rheological behavior would emerge in response to changes not only in shear rate but also in the degree of shear strain (%). To investigate this, the shear rate was maintained at 1 rad/s, while the shear strain was varied from 10 to 6000%. During this process, the values of both storage modulus ($G'$) and loss modulus ($G''$) were carefully monitored. Interestingly, a trend was observed where $G'$ and $G''$ initially increased and then decreased sequentially. Up to about 198% shear strain, both $G'$ and $G''$ increased, and after 198%, they decreased (Figure 3b, black). It is noteworthy that no corresponding changes in shear-strain-dependent behavior were detected when testing PVA alone (Figure 3b, gray). Thus, when considering the results shown in Figures 2 and 3, the PVA/TA complex units in the dilute phase, *l*-VATA, become associated with each other. This association is facilitated by TA molecules in response to vortex or shear forces that are decorated on the surface the complexes. This process leads to an enhancement in overall solution characteristics, including properties such as viscosity, storage, and loss moduli. However, when extreme shear rate or shear strain is introduced, the bonding between the PVA and TA exhibits reversible characteristics; consequently, the PVA/TA complex dissociates, resulting in a reduction in the overall viscosity and rheological properties (Figure 3c).

Cytotoxicity assays were conducted given its water-like formulation and robust adhesive properties. Equivalent concentrations of PVA (10.15 wt %) and TA (1.62 wt %) were individually added to the media for comparison. The concentrations were verified through GPC for PVA and UV−vis spectroscopy for TA (as shown in Figure S1a,b). A phosphate-buffered saline (PBS) solution served as the negative control. After 24 h of incubation, both LIVE/DEAD assays and CCK-8 quantifications were carried out. Remarkably, the number of dead cells (indicated in red) did not show a significant decline, nor did the cells change into a round morphology up to 1.5 $\mu$L (Figure 4a). We observed that the cytotoxicity of TA alone was effectively mitigated when complexed with PVA. Cell viability data showed that *l*-VATA exhibited higher percentages of viable cells compared to TA alone at various concentrations (Figure 4b). Specifically, viability was 115 ± 13% for *l*-VATA, 93 ± 4% for TA (0.25 $\mu$L); 103 ± 2% for *l*-VATA, 92 ± 4% for TA (0.5 $\mu$L); 88 ± 9% for *l*-VATA, 73 ± 10% for TA (1 $\mu$L); 57 ± 10% for *l*-VATA, and 41 ± 30% for TA (1.5 $\mu$L).

The bottom, dense phase of polyphenolic coacervate faces challenges in transferring from bulk VATA material to the surface and in spreading across the surface, as illustrated in Figure 5a. Conversely, the dilute phase, *l*-VATA, offers a significant advantage: although its chemical composition resembles that of the dense phase, its lower viscosity facilitates ease of handling when employed as an adhesive. This characteristic allows *l*-VATA to be readily applied to microsize curvature materials such as human hair. To demonstrate this, human hair strands thinly coated with *l*-VATA were used to test the adhesive force attached between hair-to-hair strands. Handling individual hair strands is a difficult task due to its thin and flexible nature, so a 30G needle was used to support a hair strand, exposing about 3 cm of it. By loading the *l*-VATA solution into the larger diameter 18G needle, the exposed hair could be dipped by inserting it into 18G needle for 1 min (Figure 5b, steps 1, 2, and 3). This process of attaching individual hair was repeated to create a total of 10 strands. They were then overlapped to form a thicker hair fiber and threaded between the handles of a binder clip, enabling the center to lift predetermined weight objects (Figure 5b). Weights of 50, 100, 200, 500, and 700 g were easily lifted, but the hair strand could not support a weight of 1200 g (Figure 5c). Upon examination of a magnified image of the hair breaking point, it was evident that the failure occurred in the plain hair portion, not in the region of the hair-to-hair attachment indicated by the dotted red box (Figure 5c, right photo). Thus, *l*-VATA demonstrated its capability to serve as an effective low-viscous glue. Its ability to spread thinly and uniformly even on localized areas, such as hair, enabled it to exhibit significant adhesive strength.

As depicted in Figure 5b, a hair fiber consisting of 10 strands could lift an object weighing at least 700 g. This study further explored the potential of *l*-VATA as an extension agent for living hair. A 2 cm long single human hair strand was dipped into a pipette tip filled with 20 $\mu$L of *l*-VATA, adhering it to mouse hair without touching the skin. After curing for 20 min, the attached human hair strand was lifted after anesthetization. Surprisingly, the strand was able to lift the whole ∼50 g mouse, revealing the strong adhesion strength (Figure 5d). In some trials, the mouse fell due to the entire mouse's hair being pulled out, not an interfacial failure between the attached strand and mouse hair (Figure 5e). These results affirm the powerful adhesive strength of a thin *l*-VATA coating even in live substrates. The low viscosity and easy spread of *l*-VATA in its dilute phase demonstrated its suitability for thin and uniform applications in localized areas, showcasing superior adhesiveness.

For further exploration into cosmetic applications, we demonstrated the feasibility of hair-to-skin attachment using *l*-VATA. To simulate human skin conditions, pork skin was utilized as the substrate and heated to 37 °C in a water bath. The tips of several human hair strands were dipped into *l*-VATA and then adhered to the pork skin. After allowing the adhesive to dry under ambient conditions for 5 min, the hair strands were successfully attached to the skin (Figure 5f, left panels). To evaluate the adhesive strength, a tweezer was employed to move the hair strands back and forth, as illustrated in Figure 5f. Although the hair strands bent due to mechanical stress, the glued root section maintained remarkable stability. However, the water-resistant adhesive capabilities of *l*-VATA were found to be inadequate for such applications. As revealed in Figure 5g, the adhesive strength of *l*-VATA on pork skin diminished after the fourth tweezer moving cycles, possibly due to the presence of an oily layer on the skin. This presents a challenge for


https://doi.org/10.1021/acsomega.3c08833
ACS Omega 2024, 9, 2953−2961

polyphenolic adhesives to achieve robust adhesion under oily environments. Notably, direct protein-to-protein (i.e., hair-to-hair) adhesion did not exhibit such failure in adhesion.

## 4. CONCLUSION

The polyphenolic coacervates have long been a subject of study with a predominant focus on their dense phase. The dilute phase, often sidelined in prior research, emerged as a novel entity of immense interest in our study. Investigating the *l*-VATA phase, we illuminated the molecular interplay that drives alterations in its viscosity, adhesion, and rheological properties under varying shear forces. Its impressive adhesive capability, even on substrates as delicate as human hair, underscores the *l*-VATA's potential in precision bonding. Furthermore, the resilience demonstrated on live substrates and human skin mimetic substrates herald significant implications for micro-engineering, biomedicine, and cosmetic application. This exploration pivots the discourse, positioning the dilute phase of coacervates, particularly *l*-VATA, as an innovative contender for future scientific endeavors.

## ■ ASSOCIATED CONTENT

### Supporting Information

The Supporting Information is available free of charge at https://pubs.acs.org/doi/10.1021/acsomega.3c08833.

Concentration calibration curves of PVA and TA, entanglement point of PVA, and hydrodynamic size calibration curves of PEG (PDF)

Demonstration of the thickness of the VATA coacervate (MP4)

Breaking point of the hair-to-hair gluing model (MP4)

Mouse lifting with a single strand of human hair (MP4)

## ■ AUTHOR INFORMATION


### Corresponding Author

**Haeshin Lee** − *Department of Chemistry, KAIST (Korea Advanced Institute of Science and Technology), Daejeon 34141, Republic of Korea; Polyphenol Factory Co., Ltd., Truth Hall (KAIST), Daejeon 34051, Republic of Korea;* orcid.org/0000-0003-3961-9727; Email: haeshin@kaist.ac.kr

### Authors

**Helen H. Ju** − *Department of Chemistry, KAIST (Korea Advanced Institute of Science and Technology), Daejeon 34141, Republic of Korea*

**Eunu Kim** − *Department of Chemistry, KAIST (Korea Advanced Institute of Science and Technology), Daejeon 34141, Republic of Korea*

**Han-Yeol Yang** − *Department of Chemistry, KAIST (Korea Advanced Institute of Science and Technology), Daejeon 34141, Republic of Korea; Polyphenol Factory Co., Ltd., Truth Hall (KAIST), Daejeon 34051, Republic of Korea*

**Yu Ri Nam** − *Department of Chemistry, KAIST (Korea Advanced Institute of Science and Technology), Daejeon 34141, Republic of Korea*

**Jingxian Wu** − *Department of Chemistry, KAIST (Korea Advanced Institute of Science and Technology), Daejeon 34141, Republic of Korea*

Complete contact information is available at: https://pubs.acs.org/10.1021/acsomega.3c08833


### Author Contributions

H.H.J. performed investigation, methodology, visualization, writing-original draft, writing-review, and editing; E.K. performed investigation, methodology, and visualization; H.-Y.Y. performed investigation and methodology; Y.R.N. contributed to software; J.W. contributed to software; H.L. contributed to conceptualization, funding acquisition, methodology, project administration, supervision, writing-original draft, writing-review, and editing.

### Notes

The authors declare no competing financial interest.

## ■ ACKNOWLEDGMENTS

This research was supported by the National Research Foundation of Korea (NRF) grants funded by the Government of Korea (MSIT): Center for Multiscale Chiral Architectures, Science Research Center (SRC) Program (2018R1A5A1025208) and the Food and Drug Administration of South Korea (21173MFDS562).

## ■ ABBREVIATIONS

| | |
|---|---|
| PVA | poly(vinyl alcohol) |
| TA | tannic acid |
| VATA | dense phase of PVA/TA coacervate |
| *l*-VATA | liquid-VATA (dilute phase of PVA/TA coacervate) |
| LLPS | liquid−liquid phase separation. |

## ■ REFERENCES


(1) Bungenberg de Jong, H.; Kruyt, H. Coacervation (partial miscibility in colloid systems). *Proc. K. Ned. Akad. Wet.* **1929**, *32*, 849−856.

(2) Mohanty, B.; Aswal, V.; Kohlbrecher, J.; Bohidar, H. Synthesis of Gelatin Nanoparticles via Simple Coacervation. *J. Surf. Sci. Technol.* **2005**, *21*, 149−160.

(3) Barthold, S.; Kletting, S.; Taffner, J.; de Souza Carvalho-Wodarz, C.; Lepeltier, E.; Loretz, B.; Lehr, C.-M. Preparation of nanosized coacervates of positive and negative starch derivatives intended for pulmonary delivery of proteins. *J. Mater. Chem. B* **2016**, *4*, 2377−2386.

(4) Hiwatari, Y.; Yoshida, K.; Akutsu, T.; Yabu, M.; Iwai, S. Polyelectrolyte-micelle coacervation: Effect of coacervate on the properties of shampoo. *Int. J. Cosmet.* **2004**, *26*, 316−316.

(5) Yuan, Y.; Kong, Z.-Y.; Sun, Y.-E.; Zeng, Q.-Z.; Yang, X.-Q. Complex coacervation of soy protein with chitosan: Constructing antioxidant microcapsule for algal oil delivery. *LWT* **2017**, *75*, 171−179.

(6) Chollakup, R.; Smitthipong, W.; Eisenbach, C. D.; Tirrell, M. Phase Behavior and Coacervation of Aqueous Poly(acrylic acid)−Poly(allylamine) Solutions. *Macromolecules* **2010**, *43*, 2518−2528.

(7) Zhao, M.; Zacharia, N. S. Sequestration of Methylene Blue into Polyelectrolyte Complex Coacervates. *Macromol. Rapid Commun.* **2016**, *37*, 1249−1255.

(8) Wang, Q.; Schlenoff, J. B. The Polyelectrolyte Complex/Coacervate Continuum. *Macromolecules* **2014**, *47*, 3108−3116.

(9) Jing, B.; Ferreira, M.; Gao, Y.; Wood, C.; Li, R.; Fukuto, M.; Liu, T.; Zhu, Y. Unconventional Complex Coacervation between Neutral Polymer and Inorganic Polyoxometalate in Aqueous Solution via Direct Water Mediation. *Macromolecules* **2019**, *52*, 8275−8284.

(10) Kim, J.-S.; Hwang, H.; Lee, D.; Lee, H. Electrospinnable Neutral Coacervates for Facile Preparation of Solid Phenolic Bioadhesives. *ACS Appl. Mater. Interfaces.* **2021**, *13*, 37989−37996.

(11) Lee, D.; Hwang, H.; Kim, J.-S.; Park, J.; Youn, D.; Kim, D.; Hahn, J.; Seo, M.; Lee, H. VATA: A Poly(vinyl alcohol)- and Tannic Acid-Based Nontoxic Underwater Adhesive. *ACS Appl. Mater. Interfaces.* **2020**, *12*, 20933−20941.

(12) Kim, K.; Shin, M.; Koh, M.-Y.; Ryu, J. H.; Lee, M. S.; Hong, S.; Lee, H. TAPE: A Medical Adhesive Inspired by a Ubiquitous Compound in Plants. *Adv. Funct. Mater.* **2015**, *25*, 2402−2410.
(13) Guo, Q.; Zou, G.; Qian, X.; Chen, S.; Gao, H.; Yu, J. Hydrogen-bonds mediate liquid-liquid phase separation of mussel derived adhesive peptides. *Nat. Commun.* **2022**, *13*, 5771.
(14) Jin, S.; Kim, S.; Kim, D. S.; Son, D.; Shin, M. Optically Anisotropic Topical Hemostatic Coacervate for Naked-Eye Identification of Blood Coagulation. *Adv. Funct. Mater.* **2022**, *32*, 2110320.
(15) Qie, R.; Moghaddam, S. Z.; Thormann, E. A Curable Underwater Adhesive Based on Poly(propylene oxide) and Tannic Acid Coacervate. *ACS Appl. Polym. Mater.* **2023**, *5*, 1646−1650.
(16) Valois, E.; Mirshafian, R.; Waite, J. H. Phase-dependent redox insulation in mussel adhesion. *Sci. Adv.* **2020**, *6*, No. eaaz6486.
(17) Wang, Z.; Zhang, S.; Zhao, S.; Kang, H.; Wang, Z.; Xia, C.; Yu, Y.; Li, J. Facile biomimetic self-coacervation of tannic acid and polycation: Tough and wide pH range of underwater adhesives. *Chem. Eng. J.* **2021**, *404*, 127069.
(18) Zhang, P.; Shen, K.; Alsaifi, N. M.; Wang, Z.-G. Salt Partitioning in Complex Coacervation of Symmetric Polyelectrolytes. *Macromolecules* **2018**, *51*, 5586−5593.
(19) Park, S.; Barnes, R.; Lin, Y.; Jeon, B.-J.; Najafi, S.; Delaney, K. T.; Fredrickson, G. H.; Shea, J.-E.; Hwang, D. S.; Han, S. Dehydration entropy drives liquid-liquid phase separation by molecular crowding. *Commun. Chem.* **2020**, *3*, 83.
(20) Li, M.; Mirshafian, R.; Wang, J.; Mohanram, H.; Ahn, K. A.; Hosseinzadeh, S.; Pervushin, K. V.; Waite, J. H.; Yu, J. Compliant Clients: Catechols Exhibit Enhanced Solubility and Stability in Diverse Complex Coacervates. *Biomacromolecules* **2023**, *24*, 4190−4198.
(21) Nielen, W. M.; Willott, J. D.; Galicia, J. A. R.; de Vos, W. M. Effect of Solution Viscosity on the Precipitation of PSaMA in Aqueous Phase Separation-Based Membrane Formation. *Polymers* **2021**, *13*, 1775.
(22) Ren, J.; Kong, R.; Gao, Y.; Zhang, L.; Zhu, J. Bioinspired adhesive coatings from polyethylenimine and tannic acid complexes exhibiting antifogging, self-cleaning, and antibacterial capabilities. *J. Colloid Interface Sci.* **2021**, *602*, 406−414.
(23) Li, L.; Hsieh, Y.-L. Ultra-fine polyelectrolyte hydrogel fibres from poly(acrylic acid)/poly(vinyl alcohol). *Nanotechnology* **2005**, *16*, 2852.


https://doi.org/10.1021/acsomega.3c08833
*ACS Omega* 2024, 9, 2953−2961